



# Discrete element modeling of the Hongshiyuan landslide triggered by the 2014 Ms 6.5 Ludian earthquake in Yunnan, China

Wei Chao Li<sup>1,2</sup> · Gang Deng<sup>1,2</sup> · Wen Cao<sup>3</sup> · Chong Xu<sup>4</sup> · Jian Chen<sup>5</sup> · Min Lee Lee<sup>6</sup>

Received: 19 July 2018 / Accepted: 8 July 2019 / Published online: 13 August 2019  
© Springer-Verlag GmbH Germany, part of Springer Nature 2019

## Abstract

The Hongshiyuan landslide was triggered by the Ms 6.5 Ludian earthquake in 2014 with more than  $1200 \times 10^4 \text{ m}^3$  of rocks displaced. The landslide deposited entirely on the valley floor, and the landslide dam was eventually converted to a hydraulic structure for a permanent disposal. Despite the importance of material compositions to the slope stability and internal stability of a landslide dam, it was practically not viable and costly to explore the deeply buried materials in field. A 2D discrete element modeling (PFC2D code) was performed in this study to investigate the kinematic behavior of the Hongshiyuan landslide. The study aims to provide insights into the material compositions of the landslide dam for future stability evaluations. The simulation results showed that for the landslide sitting in a deep V-shaped valley with constrained movement and steep slip surface gradient, the kinematic behavior was more sensitive to the bond strength (strength of intact rock mass) than the residual friction coefficient (residual friction of detached rock mass). The simulation results also suggested that the rock blocks were scarcely decomposed during sliding, as the material compositions of the landslide dam was primarily controlled by the development of joints and fissures prior to the failure.

**Keywords** Earthquake-triggered landslide · Landslide dam · Discrete element method · Kinematic behavior · Hongshiyuan landslide · Ludian Earthquake

## Introduction

A strong (Ms 6.5) earthquake struck the Ludian county, Yunnan Province, China on 3rd August 2014, at 16:30 local time (Fig. 1a, b). The 2014 Ludian earthquake had affected 1.08 million people and caused 617 deaths, 112 missing, and 3143 injured (Chang et al. 2016; Li et al. 2015b; Shi et al. 2017). Thousands of landslides were triggered by the earthquake (Fig. 1c), among which the Hongshiyuan landslide was one of the largest in terms of the sliding mass volume. The Hongshiyuan landslide was deposited entirely on the valley floor with a higher deposition on the opposite bank. The deposition dammed the Niulanjiang river (Figs. 2, 3), and threatened the safety of the public at the downstream areas. The landslide dam was 83–96 m in height, 307 m in length, and 262 m in width, resulting in a total volume of about  $1200 \times 10^4 \text{ m}^3$  (Wang et al. 2015). Eventually, the landslide dam was converted to a hydraulic structure for a permanent disposal.

Owing to the massive sliding volume and the potential hazard of landslide dam breaching, extensive studies including statistical analysis, site investigation and numerical

✉ Wei Chao Li  
liwc@iwhr.com

<sup>1</sup> State Key Laboratory of Simulation and Regulation of Water Cycle in River Basin, Beijing 100048, China

<sup>2</sup> Department of Geotechnical Engineering, China Institute of Water Resources and Hydropower Research, Beijing 100048, China

<sup>3</sup> Tianjin Urban Construction Design Institute, Tianjin 300122, China

<sup>4</sup> Key Laboratory of Active Tectonics and Volcano, Institute of Geology, China Earthquake Administration, Beijing 100029, China

<sup>5</sup> School of Engineering and Technology, China University of Geosciences (Beijing), Beijing 100083, China

<sup>6</sup> Department of Civil Engineering, Faculty of Science and Engineering, University of Nottingham Malaysia, 43500 Selangor, Malaysia

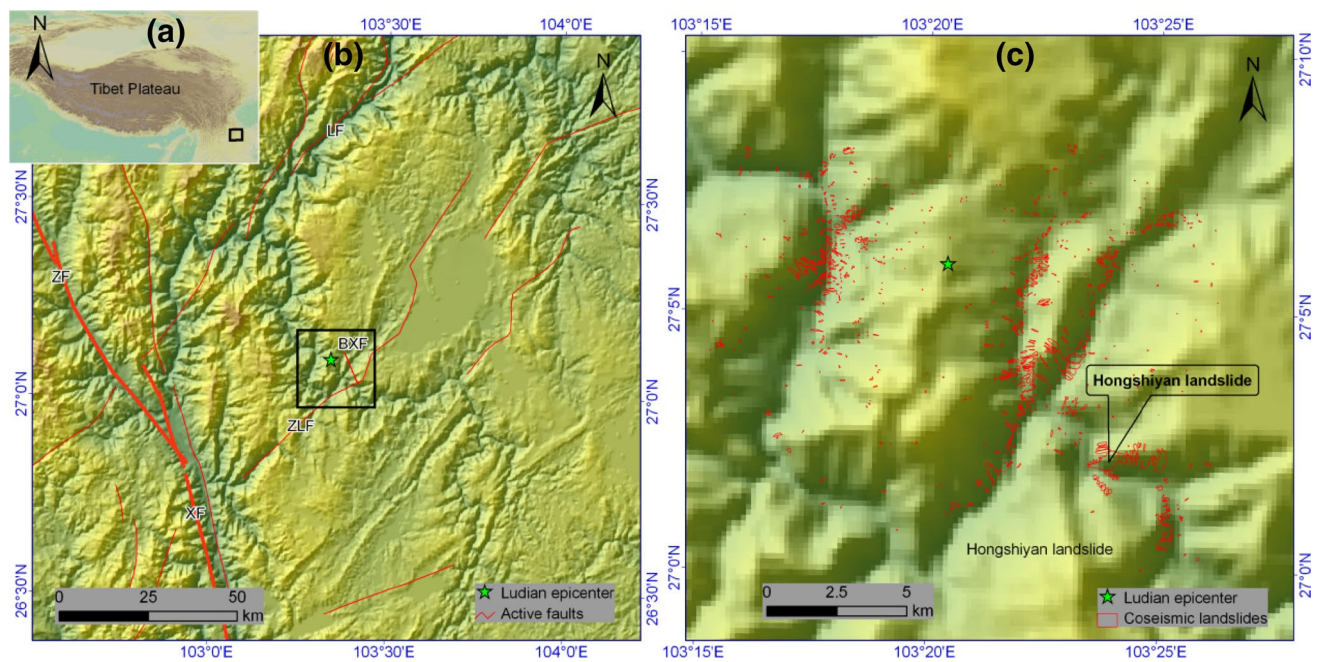


**Fig. 1** Geological setting and coseismic landslides related to the Ludian earthquake, China on 3 August 2014. **a** Location of the study area. **b** Active faults (Xu et al. 2015c, 2016b) of the study area and the Ludian earthquake epicenter, ZF-Zemuhe fault, XF-Xiaojiang

fault, LF-Lianfeng fault, ZLF-Zhaotong-Ludian fault, BXF-Baogunao-Xiaohe fault. **c** Distribution map of the coseismic landslides triggered by the Ludian earthquake and the location of the Hongshiyuan landslide (Xu et al. 2014a)

analysis had been carried out to investigate the mechanism of the Hongshiyuan landslide. Based on the distribution and geomorphologic characteristics of the Ludian earthquake, previous statistical analysis suggested that shallow hypocenter of the Ludian earthquake (Xu et al. 2014a) and local topography (Chen et al. 2015; Zhou et al. 2016) had a substantial influence on the mechanism of the landslide occurrence. Through post-failure site investigations, Chang et al. (2016) identified four factors that had contributed to the Hongshiyuan landslide, namely recent crustal deformation, combined structures, its location near to an active fault, and strong ground shaking of the Ludian earthquake. Numerical analyses had been carried out by several researchers to provide more insights into the failure mechanisms, i.e., Liu et al. (2016) using finite element method, Lv et al. (2017) using dynamic finite difference method, and Xu et al. (2017) using material point method. Based on these simulation results, the shear strength parameters of rock mass were back analyzed (Liu et al. 2016), the response of the Hongshiyuan slope before failure was studied (Lv et al. 2017), and the sliding process was simulated (Xu et al. 2017). Both the regional and local analyses above suggested that the earthquake load and local topography were the two dominating factors contributing to the failure.

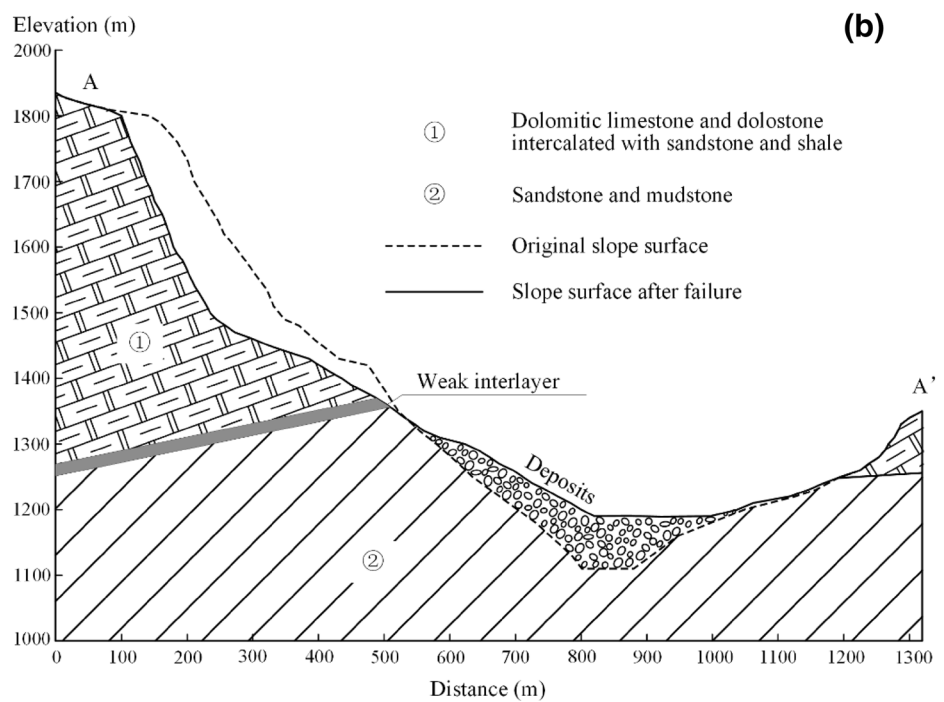
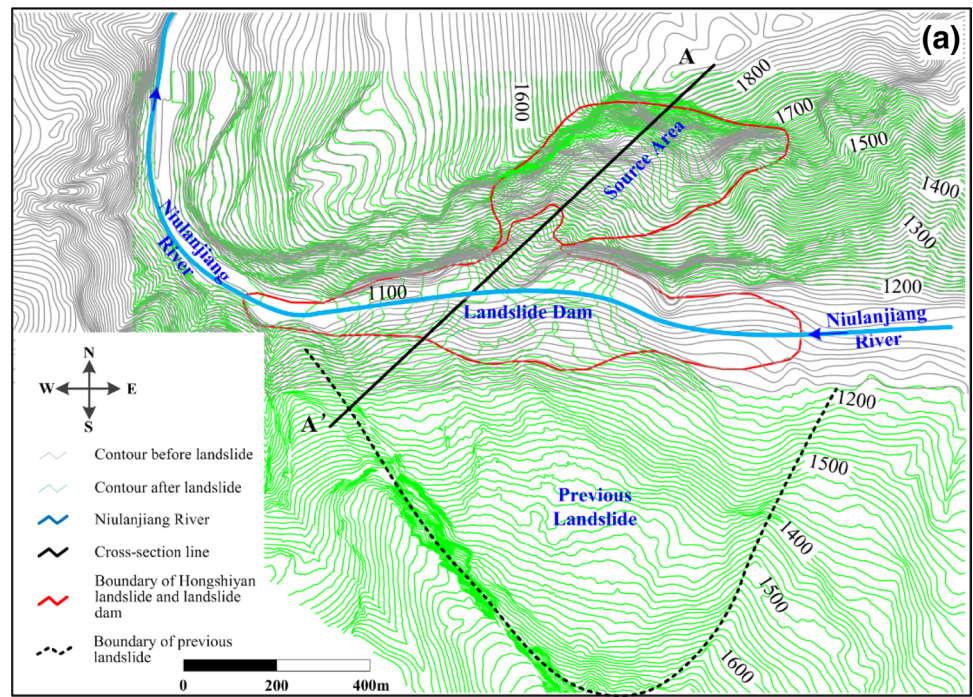
Despite of the extensive studies carried out pertaining to the case study of the Hongshiyuan landslide as cited above, most of the studies focused mainly on the failure

mechanism. Studies on the kinematic behavior of the landslide are still very limited. Xu et al. (2017) simulated the sliding process using the material point method. However, their work focused mainly on the modeling approach using a three-dimensional model, whereas the Hongshiyuan landslide was only taken as a case study to show the validity of the proposed approach. The kinematic behavior and sliding process of the landslide were not investigated explicitly in their reported study.

The kinematic behavior of earthquake-triggered landslides are rarely monitored or measured in field attributed to their sudden failure or rapid movement characteristics. It is difficult to analyze the dynamic sliding mechanisms based on the field observation alone (Havenith et al. 2003). Numerical modeling tools such as discrete element method (DEM), discontinuous deformation analysis (DDA), material point method (MPM) have been widely used as alternatives to give insights into the dynamic processes (Tang et al. 2009; Wu et al. 2009; Soga et al. 2016; Xu et al. 2017).

In recent years, many numerical studies have been conducted using the discrete element method to investigate the dynamic processes of earthquake-triggered landslides. For instances, Tang et al. (2009) investigated the kinematic behavior of the catastrophic Tsaoling landslide triggered by the Chi-Chi earthquake, Li et al. (2012a), Zhou et al. (2013a, b), Yuan et al. (2014), and Deng et al. (2017) simulated the Donghekou landslide, Yangjiagou landslide, and

**Fig. 2** The Hongshiyuan landslide: **a** topographic map showing the elevation and affected area of the landslide before and after failure (modified from KECL and Zhaotong Water Survey 2014); and **b** slope profile before and after failure (modified from Li et al. 2015a)



Wenjiagou rock avalanche triggered by the Wenchuan earthquake, respectively. These simulations showed the advancement of discrete element method in modeling the complicated seismically induced dynamic processes, such as bending, cracking, disintegrating, block tilting, ejecting and slipping (Havenith et al. 2003; Tang et al. 2009; Wasowski et al. 2011; Li et al. 2012a; Yuan et al. 2014; Deng et al. 2017). The validity of the input slope material

properties is paramount to the validity of the simulation results (Wasowski et al. 2011). Trial-and-error approach was usually adopted to calibrate the input parameters to yield realistic outputs. Most of the previous studies pertaining to the topic focused on the dynamic processes, and the results suggested that a low residual friction coefficient played a key role in inducing a long distance movement. However, studies on the composition of deposition, which is essential to the

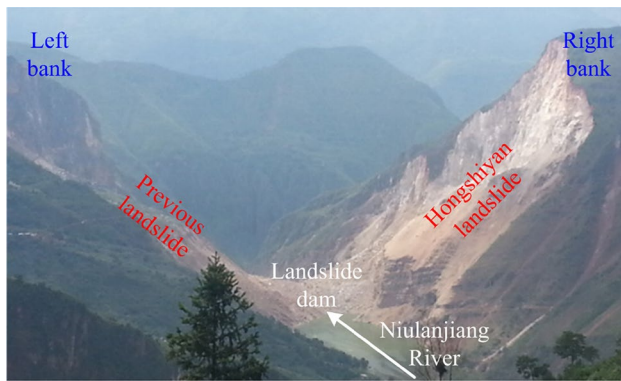


**Fig. 3** Locations of the Hongshiyuan landslide and the previous landslide (modified from KECL and Zhaotong Water Survey 2014)

slope stability and internal stability of a landslide dam, have been scarcely investigated by numerical modelling.

Considering that limited studies are available on the kinematic behavior of the Hongshiyuan landslide and the importance of material compositions to the stability of a landslide dam, this study aims to simulate the kinematic behavior of the landslide through a 2D discrete element modeling with parametric study. The simulation results are used to interpret the material compositions of the landslide dam for future stability evaluations. Although the discrete element method has limitations in quantitatively investigating the material compositions of the landslide dam, the work demonstrates that it can provide useful insights for interpreting the material compositions qualitatively.

## Background of study area

### Tectonic setting and the Ludian earthquake

The Qinghai Tibet Plateau was formed as the result of subduction of the Indian plate under the Eurasian plate (Molnar and Tapponnier 1975; Tapponnier and Molnar 1977; Tapponnier et al. 1986, 2001). At present, this crustal movement is still active, and hence several major earthquakes occurred at both the interior and surrounding areas of the Qinghai Tibet Plateau. A large number of landslides had been triggered by these earthquakes, such as the Kashmir earthquake in 2005 (Kaneda et al. 2008; Owen et al. 2008), the Wenchuan earthquake in 2008 (Xu et al. 2009, 2014c), the Lushan earthquake in 2013 (Xu et al. 2013, 2015a, b), the Minxian earthquake in 2013 (Xu et al. 2014b; Tian et al. 2016), the Ludian earthquake in 2014 (Fang et al. 2014; Xu et al. 2014c, 2015c; Zhang et al. 2014a, b) and the Nepal earthquake in 2015 (Avouac et al. 2015; Kargel et al. 2016; Xu et al. 2016a).

The Ludian earthquake occurred in the southeastern region of the Qinghai-Tibet Plateau (Fig. 1a). The epicenter coordinates were 27.0994 N and 103.34 E. The magnitude of the Ludian earthquake was Mw 6.2 according to the United States Geological Survey (USGS) and Mw 6.5 according to the China Earthquake Networks Center (CENC). The main active faults in the region, located 50 km away from the earthquake epicenter, were known as Zemuhe fault and Xiaojiang fault. These two faults were oblique and both made of NNE striking. In addition, a number of parallel strike-slip faults were developed in this area including Lianfeng fault and Zhaotong-Ludian fault which were located 40 km and 10 km away from the earthquake epicenter, respectively. There were a series of small sub-faults developed between the two active faults. Seismic geological survey, aftershock distribution and post-earthquake rupture process analysis showed that the seismogenic structure of the Ludian earthquake was originated from one of these sub-faults, namely Baogunao-Xiaohe fault (Fig. 1b) (Fang et al. 2014; Zhang et al. 2014a, b; Xu et al. 2015c).

### Coseismic landslides

The Ludian earthquake had triggered at least 1024 landslides with the area of each event  $> 100 \text{ m}^2$  (Fig. 1c), and resulted in a total landslide affected area of about  $5.19 \text{ km}^2$ . The Hongshiyuan landslide, which was located at about 9 km southeast of the earthquake epicenter (Fig. 1c), was one of the largest landslides triggered by the Ludian earthquake. The landslide occurred on the right bank of the Niulanjiang River nearby the Hongshiyuan Village, and deposited into the Niulanjiang River with a previous landslide deposit on the opposite bank (Figs. 2a, 3).

### Previous landslide on the left bank

A previous landslide was observed on the left bank (opposite the Hongshiyuan landslide) of the Niulanjiang River (Figs. 2a, 3, 4). The previous landslide has a base width and a height of about 1200 m and 900 m, respectively, resulting in a total volume of about  $5.67 \times 10^7 \text{ m}^3$  and an average thickness of 70 m (Chang et al. 2016). The previous landslide was mainly composed of gravel and stone with silt and clay filling in the voids between the coarse particles. The slope gradients above and below 1400 m elevation of the slope were  $18^\circ$  and  $36^\circ$ , respectively (Fig. 2). After the Ludian earthquake, the amount of rocks rolling down the slope was insignificant and the slope geometry has generally remained unchanged (KECL and Zhaotong Water Survey 2014).

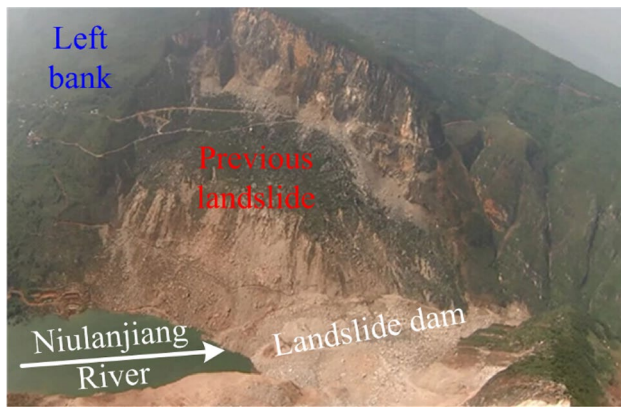


**Fig. 4** Photo of the previous landslide (modified from KECL and Zhaotong Water Survey 2014)

## Hongshiyuan landslide and landslide dam

### Geological setting

The Hongshiyuan landslide is located in Lijiashan, Ludian County. At the study area, Niulanjiang River crossed through a deep and steep V-shaped valley. The elevation of the area above the river bed was about 1100–2000 m. The gradient and height of the slope on the left bank were 35°–50° and 200–220 m, respectively (Chang et al. 2016). On the right bank, the slope gradient before failure was about 70°–85°, and the height was about 800 m. The Hongshiyuan landslide occurred at the elevation of 1300–1800 m on the right bank of the hill.

The geological profile of the region consisted of medium bedded dolomitic limestone and dolostone intercalated with sandstone and shale of Ordovician, Silurian, Devonian, and Permian systems (Chang et al. 2016). Joints, fissures and intensely weathered surfaces were developed extensively in this region as the results of intense fault development, unloading cracks, and broken rocks characterizing the upper part of the slope (Chang et al. 2016). Three sets of joints were found in the rock on the slope, i.e., steep joints at the direction normal to the river (30°NW/80°NE), joints parallel to the river (3°EW/80°S–83°S), and interbedded joints (20°NE–60°NE/10°NW–303°NW) (Chang et al. 2016). The weathering depth perpendicular to the slope on the right bank was 20–25 m (Chang et al. 2016).

### Site investigation

A landslide dam was formed in the Niulanjiang river following the Hongshiyuan landslide. The total volume of the landslide dam was about  $1200 \times 10^4 \text{ m}^3$  with a height of 83–96 m. The crest of the landslide dam was saddle-shaped with a length and a width of about 307 m and 262 m, respectively.

The dam abutment on the right side (1240 m) was higher than that of the left side (1222 m). The base width of the landslide dam along the river was about 910 m. The average upstream and downstream slope gradients were about 1:2.5 and 1:5.5, respectively (Wang et al. 2015).

According to the lithology, preliminary investigations by KECL and Zhaotong Water Survey (2014) suggested that the surface layer of the landslide dam contained mainly coarse particles with the maximum particle size was larger than 5 m. The compositions of particles > 50 cm, 2–50 cm, and < 2 cm were 50%, 35% and 15%, respectively. The amount of water leaking through the landslide dam was considerably small and clean, and hence it was deduced that the soil particles below the elevation 1180 m was well-graded with a high density (KECL and Zhaotong Water Survey 2014).

The topography and geometry of the slope on the right bank were altered significantly after the landslide. The landslide resulted in a 500 m high scar. The upper part of the slip surface was almost vertical, and the maximum height was about 350 m. The lower part of the slip surface was more gentle than the upper part (Fig. 2b).

Unloading cracks were developed extensively within 60 m to the crest of the landslide scarp. The cracks were extended mainly parallel to the river, and the average crack spacing was about 5 m. The largest crack was 30–40 cm wide, 15 m long, and the visible depth was about 1–1.5 m. The longest crack was 10–15 cm wide, and 60 m long with the same visible depth as the former (KECL and Zhaotong Water Survey 2014).

## Discrete element modelling

### Discrete element method

The kinematic behavior of the earthquake-induced Hongshiyuan landslide was simulated by the discrete element method using Particle Flow Code in two dimensions (PFC2D) (Itasca 2015). Balls and walls are the two basic elements in the PFC2D. In the discrete element method, the global behaviors of balls and walls are connected by a network of contact, and the positions and contacts between balls or between ball and wall are updated iteratively by the contact forces based on the laws of motion and force–displacement, as illustrated in Fig. 5. The detailed explanation on the theories of the discrete element method can be referred to Cundall and Strack (1979). The discrete element method was initially developed to model the rock block system (Cundall 1971; Cundall and Strack 1979). Recent trends showed that the method was increasingly common to be used for investigating the movement process of landslides as proven by its

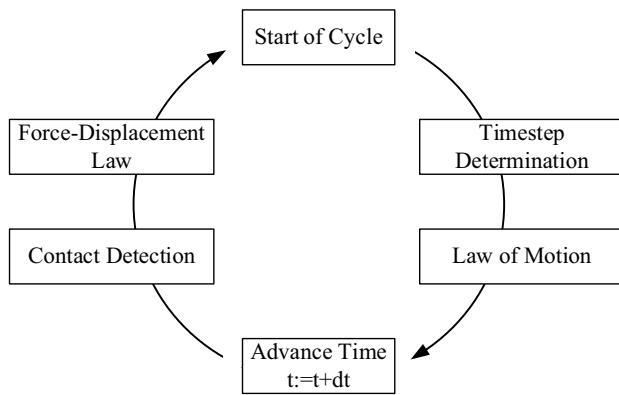


**Fig. 5** Iterative calculations in the PFC (Itasca 2015)

reasonable prediction of post-failure behavior (Tang et al. 2009; Li et al. 2012a; Lu et al. 2014; Deng et al. 2017).

### Numerical model

With the advancement in computer and software technology, 3D modeling has been undeniably preferred over 2D modeling in landslide movement simulation as the 3D modeling enables simulations of lateral spreading of mass movements. More kinetic energy is expected to be dissipated in the 3D case (Tang et al. 2009; Li et al. 2012b; Zhang et al. 2019). However, the 3D modeling strictly requires the availability of high quality input data (both resolution and accuracy), particularly the detailed topography of the pre-/post-failure of the site to identify the boundary of the sliding mass, the deposit shape and the detailed descriptions of the occurrence phenomenon (Crosta et al. 2004; Pirulli et al. 2007; Li et al. 2012b). The 2D modeling still offers several advantages over the 3D modeling in the aspects of reducing the modeling and computing time, and the possibility of interpreting the simulation results in a much more straightforward way (Itasca 2015). Numerous studies suggested that there were no significant differences in the simulated mass movement between the simpler 2D modeling and the more sophisticated 3D modeling if the modeling is calibrated carefully (Staron 2008; Tang et al. 2009; Zhang et al. 2019). The main source of discrepancy comes from the differences between the 3D actual configured geometry and the geometry on a 2D plane in the numerical model (Tang et al. 2009). PFC in two dimensions (PFC2D) was commonly adopted for the study of mechanical behavior of earthquake-triggered landslides, when possible (Tang et al. 2009; Li et al. 2012a; Zhou et al. 2013a, b; Lu et al. 2014; Yuan et al. 2014; Deng et al. 2017). The above reported studies asserted a fact that the 2D simulation could give reasonable predictions to investigate the 3D real cases in spite of some simplifications. For these reasons, the 2D modeling was adopted in the present study.

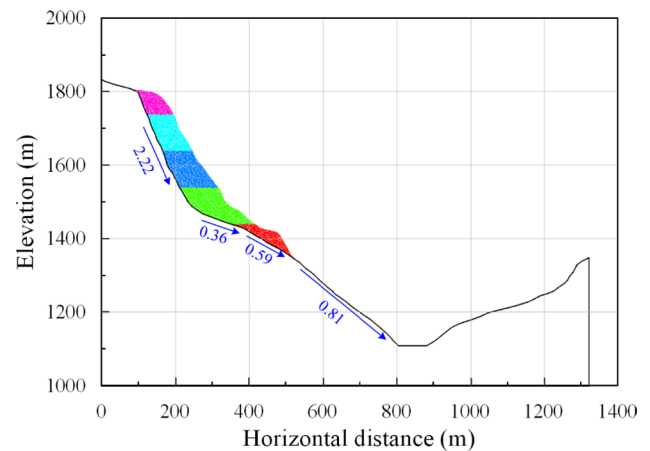


**Fig. 6** Numerical model of the Hongshiyuan landslide with different colors according to the actual field geometry

Figure 2a shows the contour of the study site before and after the Hongshiyuan landslide. The two contours are overlapped in Fig. 2a to reveal the topographical changes after the Hongshiyuan landslide. The detached mass and the slip surface along the main slide direction were validated based on the changes in contours and site investigations, as shown in the cross-section of A–A' (Fig. 2b). Since the slip surface was affirmed, the smooth bottom model was selected (Li et al. 2012b) in which the slip surface was modeled by wall elements, and the sliding mass was modeled by 8694 ball elements with radiuses of 0.5–1.5 m. To provide a clear presentation for the movement scenarios, the particles at every 100 m elevation interval were assigned with different colors, as shown in Fig. 6.

According to the site investigation, the sliding mass consisted of mainly rocks, and hence the linear parallel bond contact model was assigned in this simulation. The linear parallel bond model was developed by Potyondy and Cundall (2004) and it has been integrated into the PFC2D. In the linear parallel bond model, rocks are represented by dense packing particles that are bonded together at their contact points. The force and moment carried by the bond between particles are denoted as the cement behavior (Potyondy and Cundall 2004). In the simulation, the bond breaks when the applied stress exceeds its bond strength, after which only the residual friction of particles exists with the dismissal of the bond strength. The breakage of bonds explicitly represents the damage of rock mass, and the broken bonds form and coalesce into macroscopic fractures (Potyondy and Cundall 2004; Chang et al. 2012). The residual friction coefficient of the grains is used to represent the residual friction of the joints in the rock mass (Tang et al. 2009; Yuan et al. 2014). With these features, numerous behaviors of rock can be reproduced, such as

elasticity, fracturing, post-peak softening and strength increase with confinement (Potyondy and Cundall 2004).

The kinematics behavior of Hongshiyuan landslide was governed by the geometry and discontinuities (e.g., bedding plane and joint) of the sliding mass. Since discontinuities are critical to the disintegration of any sliding mass, it is always favorable to simulate the discontinuities directly into a model for the mass movement simulation (Huang et al. 2015; Zhang et al. 2019) when comprehensive statistical data of the discontinuities is available. However, for high and steep slopes like the present case study, it was difficult to obtain these data from the field. Therefore, the influence of discontinuities was taken into account indirectly by introducing a calibrated bond strength into the simulation. The same approach has been adopted by numerous previous studies and the simulation results reasonably reflected the actual kinematics behavior of landslides (Tang et al. 2009; Li et al. 2012a; Chang et al. 2012; Lu et al. 2014; Yuan et al. 2014; Deng et al. 2017; Scaringi et al. 2018; Zhao and Crosta 2018). In these previous studies, the calibrated bond strengths from the actual deposits were usually lower than those calibrated from the intact rock samples, and this reduction of bond strength implied the effect of discontinuities on the strength of the rock mass.

### Numerical damping

Damping is not a parameter explicitly related to any physical mechanisms. It is only used in the PFC to dissipate the energy of particles or walls to establish an equilibrium condition in a simulation. For a steady-state motion, damping is

usually set to 0.7, and no erroneous on the equilibrium forces arise (Cundall and Strack 1979; Poisel and Preh 2008; Itasca 2015). For an accelerating motion, such as the movement of landslide, damping may reduce the acceleration or the velocity of particles. The damping should be set to zero or to a reasonably small value. Therefore, the damping was set to 0.7 in the uniaxial compression test simulation. For the movement simulation, the damping was initially set to 0.7 to obtain the initial equilibrium state of the slope before failure, and subsequently set to 0 when applying the seismic load. This implied that the Hongshiyuan landslide was a seismic load and gravity driven movement, and the drag force on the movements caused by air was assumed to be negligible (Teufelsbauer et al. 2009).

### Boundary conditions

The bottom and both side boundaries were modeled in accordance with the slip surface and terrains before the slope failed. Wall elements were set along these boundaries (Fig. 6). The sliding mass, which was modeled by the ball elements, was permitted to move along the wall elements, but not crossing it.

A seismic motion was applied to the wall boundary after a primary gravitational stress field was generated (Deng et al. 2017). As suggested by Tang et al. (2009) and Yuan et al. (2014), the seismic motion was applied in terms of velocities based on the integrated acceleration records obtained from the Longtoushan seismic station for the Ludian earthquake. Figure 7 shows the integrated velocity diagram. The velocities in Fig. 7a, b, d were directly integrated from the

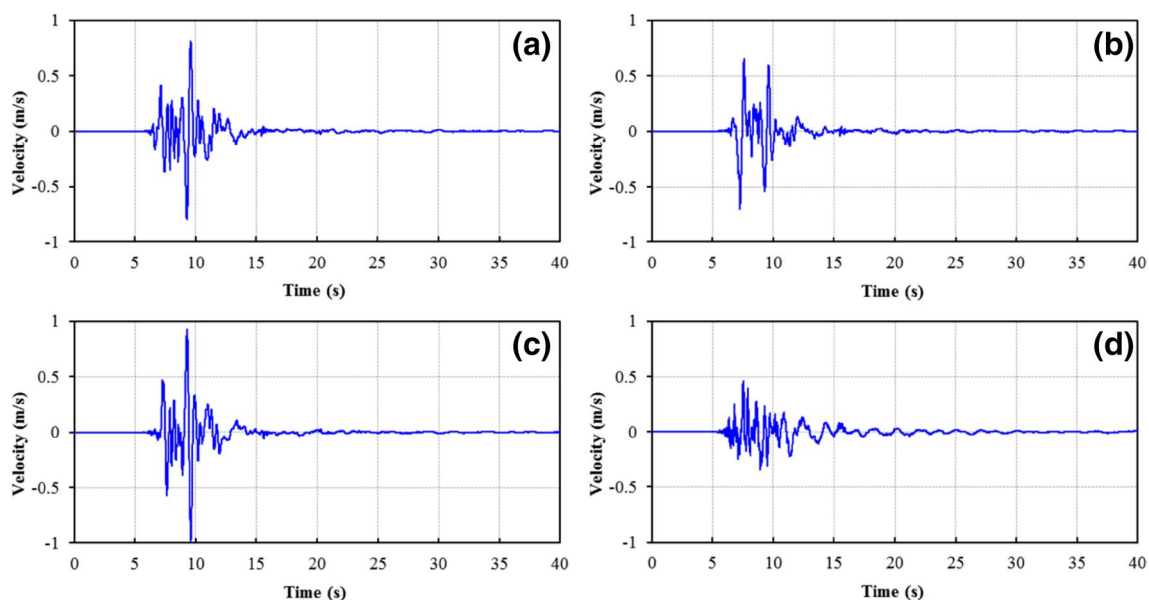


**Fig. 7** Velocity diagram by integrating the acceleration of the Longtoushan seismic station recorded for the Ludian earthquake: **a** E–W component; **b** N–S component; **c** horizontal component along the slip direction of the Hongshiyuan landslide; and **d** vertical components

**Table 1** Physical properties of the rock blocks from landslide dam (KECL and Zhaotong Water Survey 2014)

Rock block	Specific gravity, Gs	Density, $\rho$ (g/cm <sup>3</sup> )	Unconfined compression strength (Mpa)	Young's modulus (Gpa)	Poisson's ratio
Calcite–dolomite	2.83	2.77	80.00	15	0.22
Dolomite	2.84	2.81	75.00	15	0.22
Limestone	2.77	2.72	85	18	0.21

measured acceleration of the corresponding directions. The horizontal velocity along the slip direction of the Hongshiyuan landslide in Fig. 7c is calculated from Fig. 7a, b. In the simulation, the horizontal velocity in Fig. 7c and vertical velocity in Fig. 7d were applied to the wall boundary simultaneously. A seismic motion duration of 40 s was adopted in this study.

### Calibration of micro-properties

For numerical simulations by PFC2D with the linear parallel bond model, the micro-properties include effective modulus, stiffness ratio, normal and shear bond strength, and Coulomb friction coefficient are difficult to be obtained directly from laboratory tests, and there is no complete theory can reliably evaluate the micro-properties from the laboratory tests. For the reasons, a calibration process is necessary for selecting the appropriate micro-properties (Tang et al. 2009; Yuan et al. 2014; Deng et al. 2017).

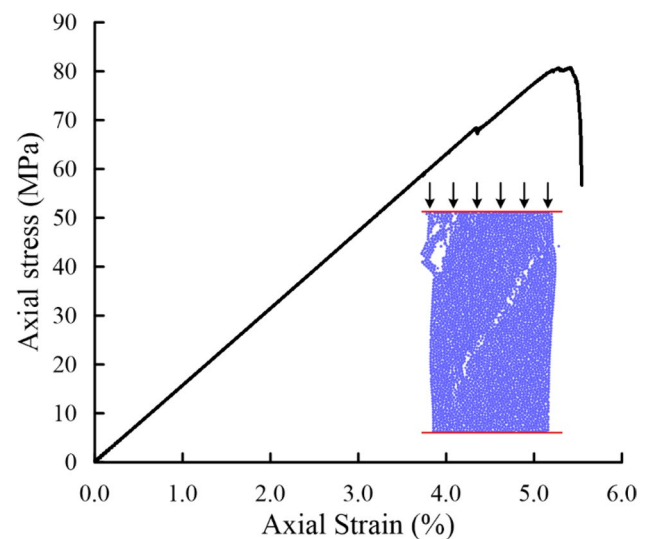
For the Hongshiyuan landslide, the detached mass consisted of fractured and weathered rocks. However, physical and mechanical properties were only tested on the intact rock blocks from the landslide dam, as tabulated in Table 1 (KECL and Zhaotong Water Survey 2014). Uniaxial compression test simulation was first performed by PFC2D to calibrate the micro-properties by referring to the test results of the rock block. Subsequently, landslide movement simulation was carried out to calibrate the micro-properties of the sliding mass by referring to the actual depositions of the Hongshiyuan landslide.

### Calibration with uniaxial compression test

A series of uniaxial compression tests were performed to fit the physical properties to those presented in Table 1 by trial-and-error. The 2D numerical model for the uniaxial compression test was 100 mm in height, 50 mm in width, and consisted of 3405 rigid disks. The disk size in the uniaxial compression test simulation is usually smaller than the disk size in the landslide simulation. However, this should not significantly affect the simulated kinematic behavior of the landslides (Tang et al. 2009; Yuan et al. 2014; Deng et al. 2017). For the linear parallel bond model, there is no definitive finding on the effect of disk size on the simulated peak strength of the granular assembly. The Young's modulus

**Table 2** Microproperties of models based on a series of uniaxial compression tests

Parameters	
Effective modulus (Gpa)	0.8
Ball stiffness ratio	1.0
Normal strength (Mpa)	40
Shear strength (Mpa)	40
Friction coefficient	1.0

**Fig. 8** Stress–strain behavior and cracked model from simulated uniaxial compression test

and Poisson's ratio were almost independent of the disk size (Potyondy and Cundall 2004). Table 2 shows the calibrated micro-properties of the models, and Fig. 8 presents the corresponding stress–strain behavior and the cracked model.

The elastic constant of Young's modulus and Poisson's ratio are two main macro-properties of rock blocks. These important parameters can be related to the micro-properties, such as effective modulus and ball stiffness ratio. Parametric simulations suggested that the effective modulus is proportional to the Young's modulus, while the Poisson's ratio is related to the ball stiffness ratio. Normal strength and shear strength are two main components of bond strength, while friction coefficient is the micro-properties of disk. Both the bond strength and friction coefficient contribute to the simulated peak strength of the rock samples from the laboratory



tests (Itasca 2015), but there is no straightforward solution to obtain these parameters. The bond strength and friction coefficient are usually calibrated according to the results from the laboratory uniaxial compression tests by trial-and-error (Tang et al. 2009; Li et al. 2012a; Yuan et al. 2014; Deng et al. 2017). This has been found to be one of the most practically efficient approach available to date (Tang et al. 2009).

Physical properties of three rock block samples were tested and summarized in Table 1 (KECL and Zhaotong Water Survey 2014). The average values of these physical properties, i.e., unconfined compression strength, Young's modulus and Poisson's ratio were used to calibrate the uniaxial compression test. Upon going through the trial-and-error process, the calibrated macro-properties were as follows: Young's modulus,  $E = 15.4$  GPa, Poisson's ratio,  $\nu = 0.22$ , and unconfined compressive strength,  $UCS = 80$  MPa. These calibrated macro-properties are reasonably identical to the mechanical properties of the rock blocks as shown in Table 1.

### Calibration with landslide deposition

Parametric simulations of the Hongshiyuan landslide were carried out to calibrate the micro-properties of the sliding mass. Table 3 shows the parameters used for calibrating the Hongshiyuan landslide deposition. The strength of the detached mass was weakened by the fractures and weathering, resulting in a lower strength than the original rock blocks. For these reasons, the parameters of bond strength and residual friction coefficient in Table 3, which was used in calibrating the landslide deposition, were lower than those calibrated from the rock block test.

Residual friction coefficient is an important parameter affecting the landslide movement. The residual friction coefficients ranging from 0.1 to 0.6 with an increment interval of 0.1 were attempted in this study. According to Tang et al. (2009) and Yuan et al. (2014), the time of applying the residual friction coefficient should be determined by Newmark's method (Newmark 1965). However, the method does not favor the estimation of critical acceleration value,

**Table 3** Parameters of landslide simulation suggested by the results of uniaxial compression test

Parameters	
Effective modulus (Gpa)	0.8
Ball stiffness ratio	1.0
Bond strength	
Normal strength (Mpa)	1, 4, 10, 40
Shear strength (Mpa)	1, 4, 10, 40
Residual friction coefficient	0.1, 0.2, 0.3, 0.4, 0.5, 0.6

which is an essential parameter for determining the application time (Jibson 2011). Furthermore, Newmark's method is suitable for landslides with shallow and stiff sliding mass (Jibson 2011), which are incompatible with the conditions of the Hongshiyuan landslide. For these reasons, the residual friction coefficient was applied immediately after the peak acceleration for simplicity. It was assumed that the detached mass slid when the peak acceleration exceeded the yield acceleration. Yuan et al. (2014) have successfully modeled the Donghekou landslide triggered by the 2008 Wenchuan Earthquake by adopting the similar approach. Other parameters including the effective modulus, stiffness ratio and density were extracted directly from the results of the uniaxial compression test simulation.

## Results and discussion

### Constraints on bond strength

In the linear parallel bond model, the strength of rock mass was simulated by the bond strength. The calibrated bond strength of 40 MPa was used to represent the initial strength of the rock blocks, while lower bond strengths of 1 MPa, 4 MPa and 10 MPa were used to simulate the extent of influences of joints and fissures on the strength of the rock mass. Parallel bond breakage is a ratio of broken bonds to the total bonds. It represents the extent of damage of sliding mass during a mass movement.

Figure 9a shows the changes of parallel bond breakage with time under different bond strengths. The evolution of parallel bond breakage can be divided into three stages as illustrated in Fig. 9b, i.e., initial stage, developing stage, and final stage. At the initial stage, the parallel bond breakage was minimal. The parallel bond breakage increased drastically during the developing stage, and eventually became stagnant at the final stage.

The duration of the initial stage was positively correlated with the bond strength as shown in Fig. 9a. For the bond strength of 1 MPa, the initial stage was practically indistinguishable as it entered into the developing stage instantly after application of the seismic load. For the bond strength of 4 MPa, it evolved into the developing stage immediately after the peak seismic acceleration. For the bond strengths of 10 MPa and 40 MPa, the developing stage was observed 10 s and 15 s after the peak seismic acceleration, respectively.

The duration of developing stage was inversely correlated with the bond strength. The higher the bond strength, the shorter the duration of the developing stage. Figure 10 shows the evolution of the landslide kinematic under different bond strengths after an elapsed time of 30 s. At this time, the fore front of all the detached masses with different bond strengths has reached the toe of the slope. Apparently, the

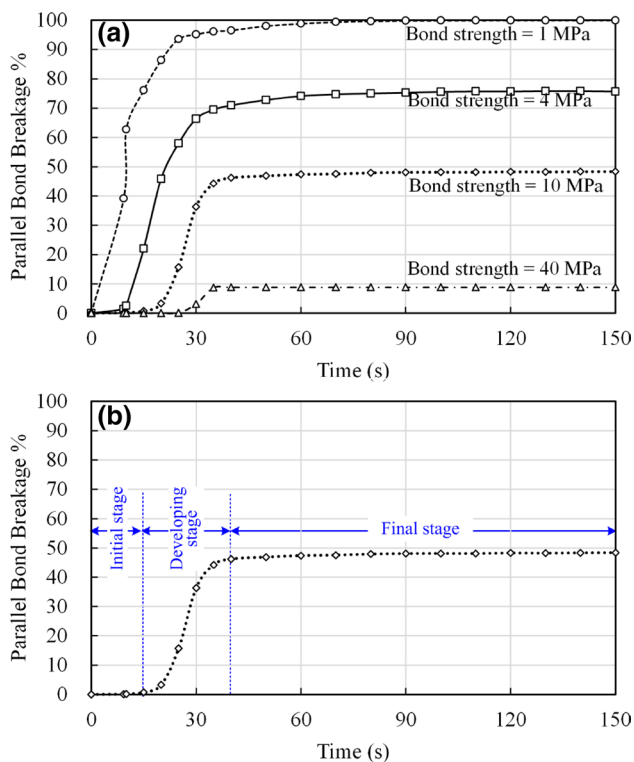


**Fig. 9** Changes of parallel bond breakage with time. **a** Under different bond strengths; **b** illustration of three stages of evolution of parallel bond breakage

detached mass with the bond strength of 1 MPa was decomposed completely, while the detached mass with the bond strength of 40 MPa almost retained its initially geometry. The detached masses with the bond strengths of 4 MPa and 10 MPa were decomposed, but largely kept their general assembly.

At the final stage, the final parallel bond breakage was inversely correlated with the bond strength, as shown in Fig. 9a. Figure 11 shows the final deposition of the detached mass after an elapsed time of 150 s under different bond strengths. The surface of the simulated depositions with the bond strengths of 1 MPa and 4 MPa were close to those shown in Fig. 4b, aside from the observation that the detached mass with the bond strength of 1 MPa was almost decomposed completely. The results with the bond strengths of 10 MPa and 40 MPa were different to those shown in Fig. 4b, and the presence of large assemblage were different to the composition of the actual deposition.

Through the parametric simulations for investigating the effect of bond strength on the evolution of landslide, the analysis results suggested that the development of fissures and joints has significantly influenced the decomposition of detached mass and the particle size distribution of the landslide deposition. By comparing the composition of the deposition revealed from the site investigation with the simulated result at the final stage (Fig. 11), the simulation result with

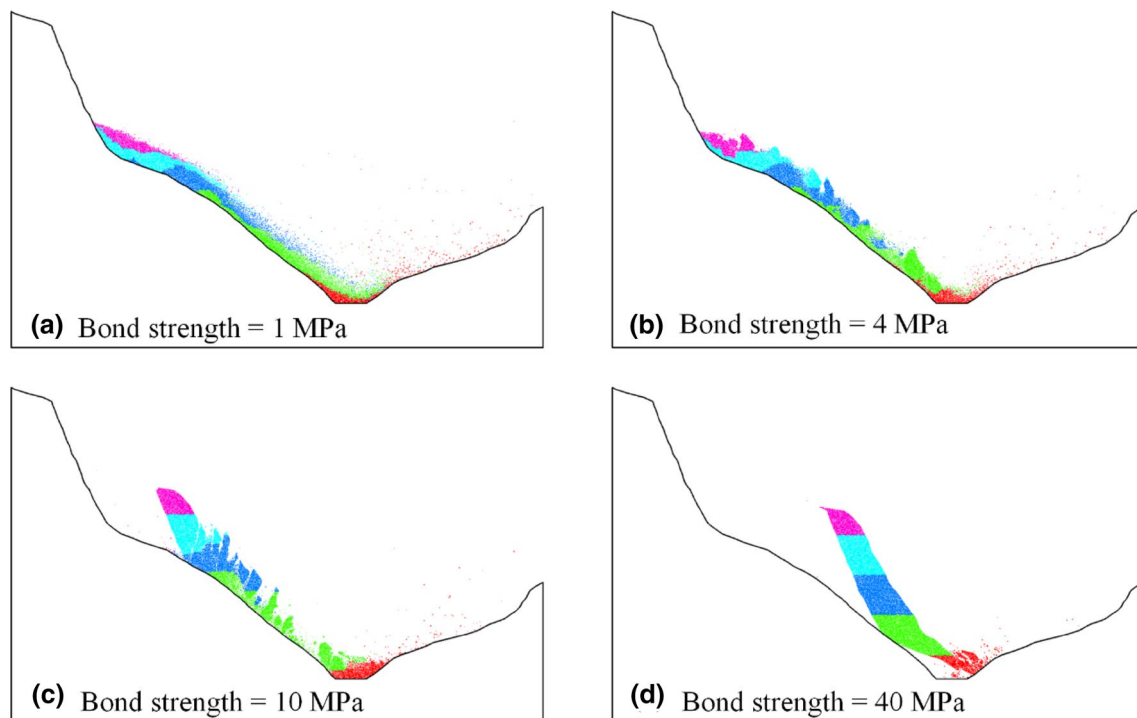


**Fig. 10** Influence of bond strength on landslide kinematics at 30 s. **a** Bond strength=1 Mpa; **b** bond strength=4 Mpa; **c** bond strength=10 Mpa; **d** bond strength=40 Mpa

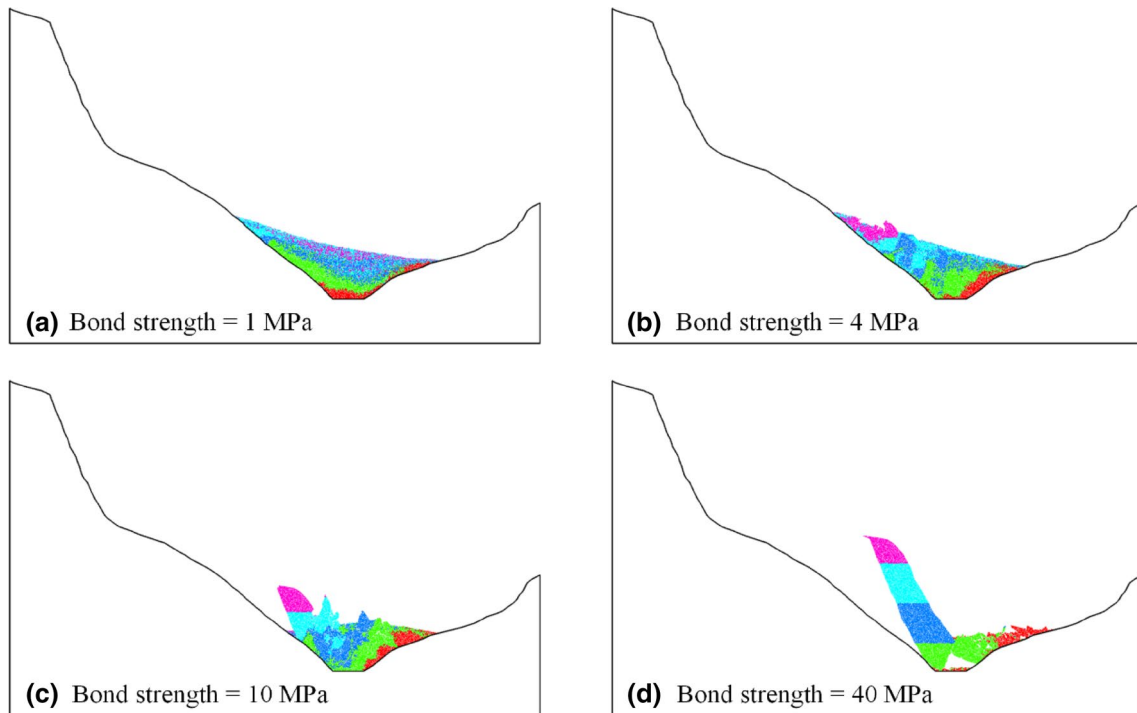


**Fig. 11** Influence of bond strength on landslide at final stage (150 s). **a** Bond strength=1 Mpa; **b** bond strength=4 Mpa; **c** bond strength=10 Mpa; **d** bond strength=40 Mpa

the bond strength of 4 MPa was reasonably identical with the actual deposition.

**Constraints on residual friction coefficients**

To investigate the constraints of residual friction coefficient on the Hongshiyuan landslide movement, 6 residual friction coefficients, i.e., 0.1, 0.2, 0.3, 0.4, 0.5, and 0.6, were attempted. It was found that no movement of detached mass was induced when the residual friction coefficient of 0.6 was applied, and hence the results of 0.6 residual friction coefficient were omitted from the subsequent analysis.

Figure 12 shows the changes of parallel bond breakage with time under different residual friction coefficients. The development of parallel bond breakage with time under the residual friction coefficients of 0.1, 0.2, 0.3, and 0.4 were fairly similar to each other. However, when the residual friction coefficient was increased to 0.5, although the final parallel bond breakage was close to those of the other four residual coefficients, the time response of the parallel bond breakage during the developing stage was visibly different (Fig. 12). After elapsed times of 15–20 s, the parallel bond breakage was inversely proportional with the residual friction coefficient (Fig. 13). The parallel bond breakage with the residual friction coefficient of 0.5 was significantly lower (about 1/5–1/4) than the other four residual friction coefficients (Fig. 13). After an elapsed time of 30 s, the parallel

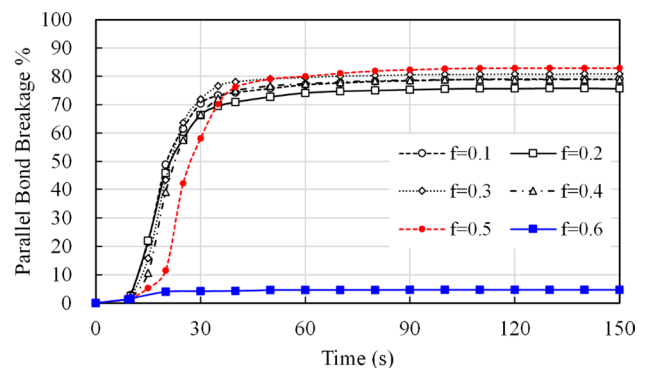


**Fig. 12** Changes of parallel bond breakage with time under different residual friction coefficients

bond breakage with the residual friction coefficient of 0.5 increased significantly to a value close to those of the other four residual friction coefficients (Fig. 13). After an elapsed time of 150 s, the parallel bond breakage with the residual friction coefficients of 0.1–0.4 were increased by about 10%. A higher increment was observed for the residual friction coefficient of 0.5, and eventually resulted in a slightly higher final parallel bond breakage than the other four residual friction coefficients (Fig. 13).

From the overall trends of the changes of parallel bond breakage with time under different residual frictional

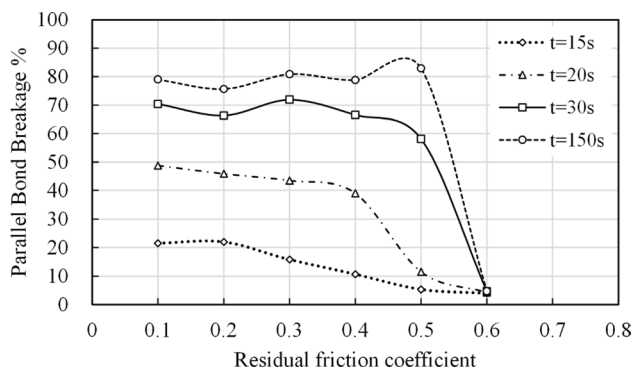


**Fig. 13** Changes of parallel bond breakage with residual friction coefficients at different time

coefficients (Fig. 12), the development of parallel bond breakage with residual friction coefficients ranging from 0.1 to 0.4 were practically invariable, while a distinguishable trend was observed for the residual friction coefficient of 0.5. Therefore, the landslide kinematics and final stage with the residual friction coefficient of 0.2 was selected (to represent the results of residual coefficients ranging from 0.1 to 0.4) for comparison with that of the residual friction coefficient of 0.5 (Fig. 14). After an elapsed time of 20 s, the detached mass with the residual friction coefficient of 0.2 was decomposed in the front, middle and rear parts (Fig. 14a), while only the front part of the detached mass was decomposed with some fractures observed in the middle part for the residual friction coefficient of 0.5 (Fig. 14d). After an elapsed time of 30 s, the decomposed detached mass with the residual friction coefficient of 0.2 laid on the slope with a considerably uniform thickness (Fig. 14b). For

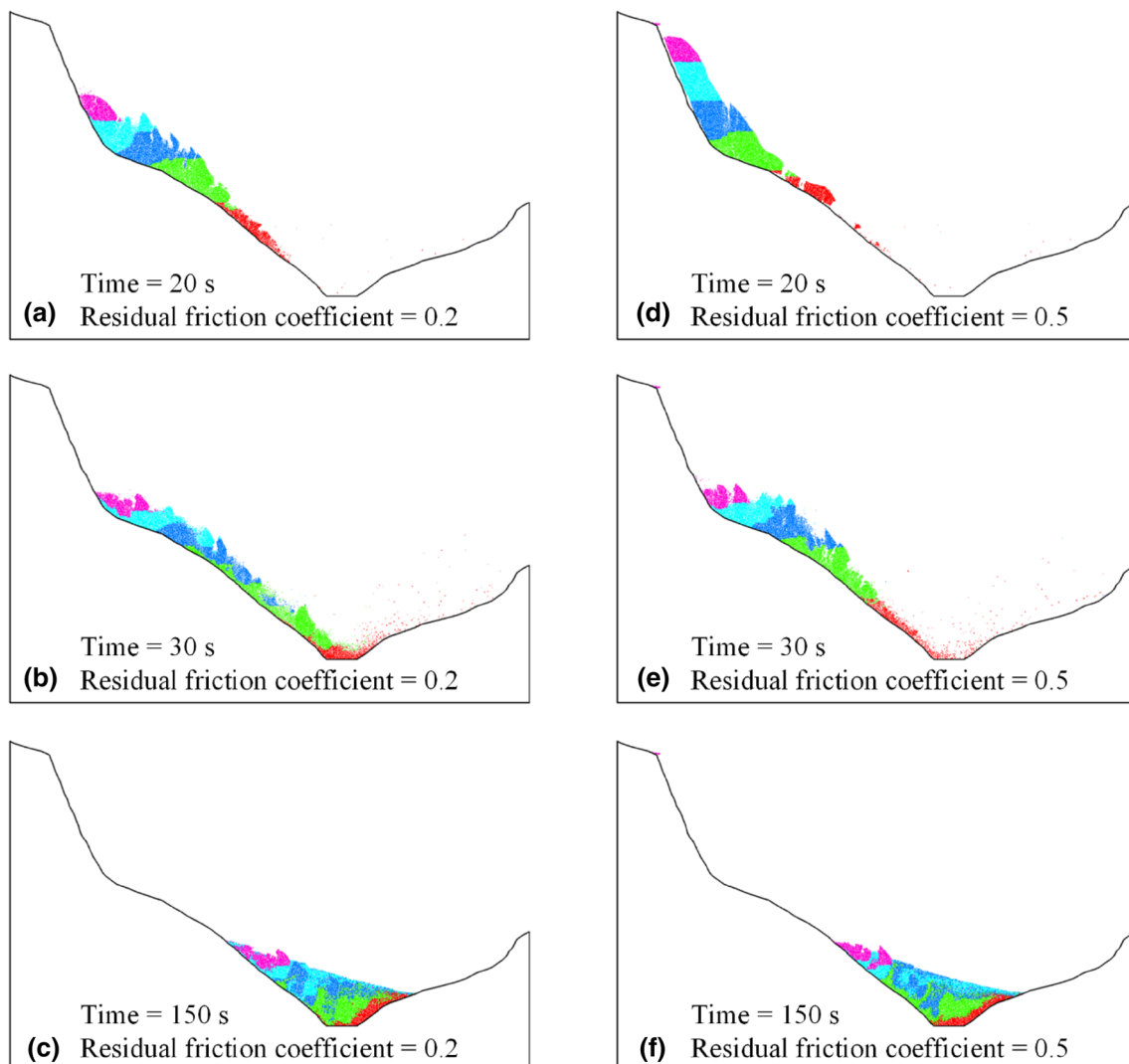


**Fig. 14** Comparison of landslide kinematics between residual friction coefficients of 0.2 and 0.5

the residual friction coefficient of 0.5, the thickness at the rear part of the decomposed detached mass was significantly greater than the front part forming an inverted triangle shape (Fig. 14e). Site investigation showed that unloading cracks were developed extensively within 60 m to the crest of the landslide scarp, and hence the rear part of the detached mass was unlikely to be remained intact and keeping the initial geometry during the initial sliding, as shown in Fig. 14d. The decomposition such as that shown in Fig. 14b was a more reasonable result. After an elapsed time of 150 s, the depositions of the detached mass for both the residual friction coefficients of 0.2 and 0.5 were reasonably similar to each other (Fig. 14c, f).

Through the parametric investigation of the effect of residual friction coefficient on the evolution of landslide, the simulated results suggested that the influences of the residual friction coefficient on the final parallel bond breakage and deposition were insignificant, but the landslide dynamics with the residual friction coefficients ranging from 0.1 to 0.4 were different from that of the residual friction coefficient of 0.5.

### Material compositions of the Hongshiyuan landslide dam

The materials composing a landslide dam play an important role in slope stability and internal stability evaluations (Swanson et al. 1986; Costa and Schuster 1988; Casagli and Ermini 1999; Casagli et al. 2003; Okeke et al. 2014). The Hongshiyuan landslide dam was converted to a hydraulic structure for a permanent disposal, and hence understanding of the material compositions would be very useful to evaluate its stability and to furnish information for the analysis and design of the hydraulic structure.

Despite the importance of the material compositions to the stability of landslide dams, it is usually difficult to obtain these data in field (Casagli et al. 2003). Drilling and pitting are usually carried out to sample the surficial materials, while exploring the deeply buried materials is costly and practically not viable. For this reason, site investigation only successfully revealed the composition of materials at the surface layer of the Hongshiyuan landslide dam, while there was no information available on the materials in the core and bottom parts of the landslide dam.

Tapping on the advantages of discrete element method in simulating landslide deposition process, it enables predictions on the composition of materials in the landslide dam. Two parameters of the Hongshiyuan landslide dam were investigated qualitatively, i.e., (i) the original location of the final deposition, and (ii) the factors controlling the particle size distribution of the materials.

To investigate the original location of the final deposition, thirteen monitoring points were located at the rear (points

1–3), middle (points 4–9) and front (points 10–13) parts of the simulated model. The original and final positions of the thirteen monitoring points are shown in Fig. 15. At the final deposition, the original front part of the detached mass was located on the opposite side bank, and it was buried by the subsequent depositions. The original middle part constituted the core of the final landslide deposition. Points 6 and 9 which were originally located at the surface layer of the middle part were deposited into the core of the deposition. The rear part of the detached mass was deposited on the rear surface of the deposition.

The grain size distributions of the mass materials of the Hongshiyuan landslide dam were deduced from the initial grain size distributions and the breakage of the detached mass after failures. Factors controlling the grain size distributions of the materials in the landslide dam can be analyzed based on the results from the parametric simulation of parallel bond breakage under different bond strengths and different residual friction coefficients.

The calibrated bond strength of 40 MPa represented the strength of the intact rock block. The final parallel bond breakage for the bond strength of 40 MPa was less than 10% (Fig. 9a), and only the front part of the detached mass was broken (Fig. 11d). This implied that the rock blocks were difficult to be broken during the moving process of the Hongshiyuan landslide, with the exception to the front part. The lower bond strengths of 1 MPa, 4 MPa and 10 MPa showed the extent of influence of joints and fissures on the strength of rock mass. With the decrease in bond strength, the parallel bond breakage increased significantly (Fig. 9a). This implied that the development of joints and fissures influenced the decomposition of the detached mass, and hence the particle size distributions of the materials significantly.

By referring to the parallel bond breakage under different bond strengths, it can be deduced that the front part of the

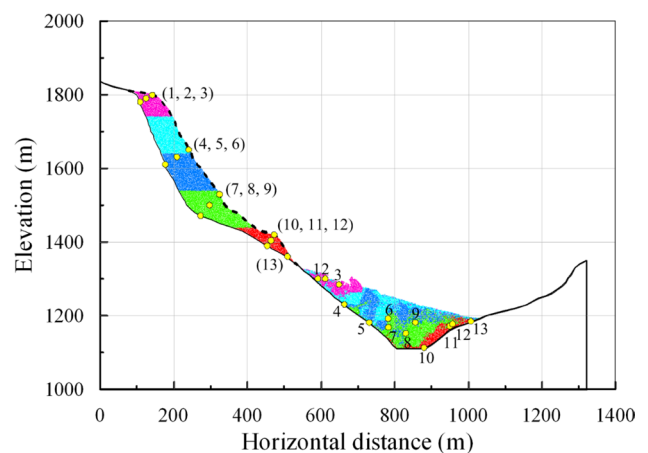


**Fig. 15** Comparison between original (on left) and final (on right) positions with 13 monitoring points

landslide was decomposed significantly and resulted in finer grain sizes. The grain size distributions at the other parts were mainly controlled by the development and density of the joints and fissures, and thus it can be evaluated qualitatively by the post-failure investigation of joints and fissures near the scarp of the landslide.

### Influence of geometry of slip surface

The parametric simulations of the earthquake-triggered Hongshiyuan landslide suggested that bond strength has a more significant influence on the final deposition than the residual friction coefficient between ball and wall. The simulation results were not sensitive to the residual friction coefficient as indicated by the simulation results of residual friction coefficients of 0.1–0.4. Other previous studies on earthquake-triggered landslides indicated that low residual friction coefficients were responsible to the observed landslide features (Wasowski et al. 2011), such as the Chi-Chi earthquake triggered Tsaoling landslide (Tang et al. 2009), the Wenchuan earthquake triggered Donghekou landslide (Li et al. 2012a; Yuan et al. 2014) and the Wenjiagou landslide (Deng et al. 2017).

The different influence of residual friction coefficient as observed in the present case study could be attributed to the gradient of the slip surface. For the cases of earthquake-triggered landslides with low residual friction coefficients, the gradient of the slip surface was relatively gentle and the run-out distance was usually long. This implied that the residual friction coefficient played a very important role on the horizontal movement of the landslide. As for the Hongshiyuan landslide, which was sitting in a deep V-shaped valley, the

opposite bank constrained the movement of the landslide. As the result, it was difficult to calibrate the residual friction coefficient accurately. The gradients of the slip surface of the Hongshiyuan landslide can be divided into 4 sections, i.e., 2.22, 0.36, 0.59, and 0.81 (Fig. 6). Considering these slip surfaces were generally greater than the residual friction coefficients, the deposition was controlled by the friction coefficient of balls and the gradient of the slip surface. The residual friction coefficient would certainly influence the momentum of a landslide, but the momentum of the Hongshiyuan landslide was difficult to be deduced from the deposition. When the slip surface gradient was greater than the applied residual friction coefficient, it was difficult to distinguish the simulated deposition purely based on the calibration of the deposition geometry.

### Dynamic response of the Hongshiyuan landslide

To interpret the dynamic responses of the Hongshiyuan landslide, the velocity and displacement in  $X$  (horizontal) and  $Y$  (vertical) directions were investigated with the monitoring particles located at the rear (points 1–3), middle (points 4–9), and front (points 10–12) parts of the simulated model (Fig. 15).

The variations in velocity with time in  $x$  and  $y$  directions are shown in Figs. 16 and 17, respectively. The velocity gradient can be defined as the acceleration of a particle. According to the Newton's second law of motion, the acceleration of a particle is controlled by the net force. Thus, the velocity gradients in Figs. 16 and 17 could also be used to represent the degree of collision interaction of a particle with the surrounding particles and walls (Li et al. 2012b).

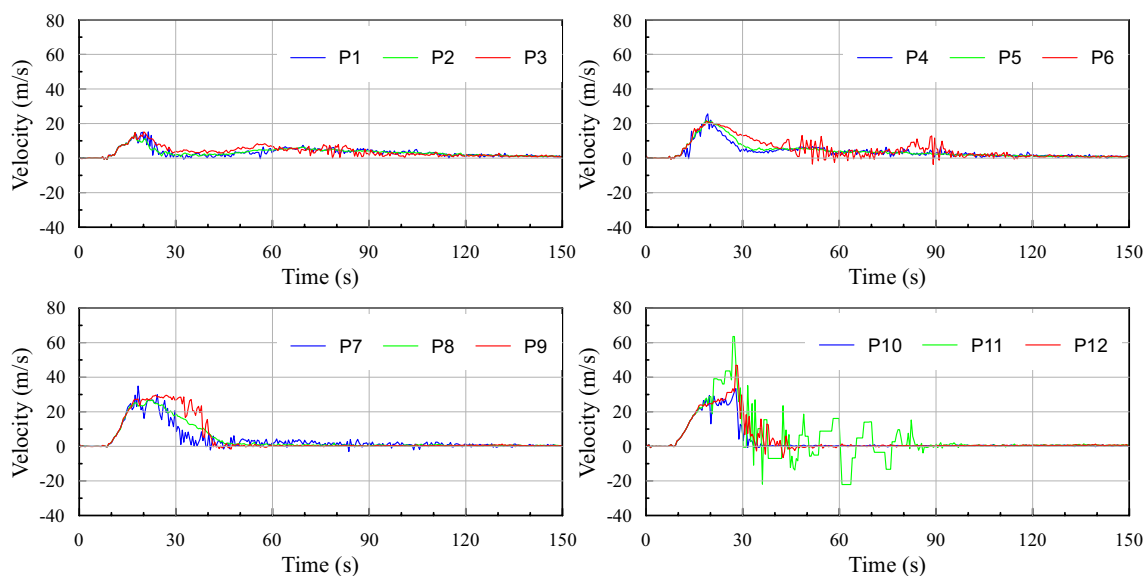


**Fig. 16** Variations of velocity in  $x$  (horizontal) direction with time

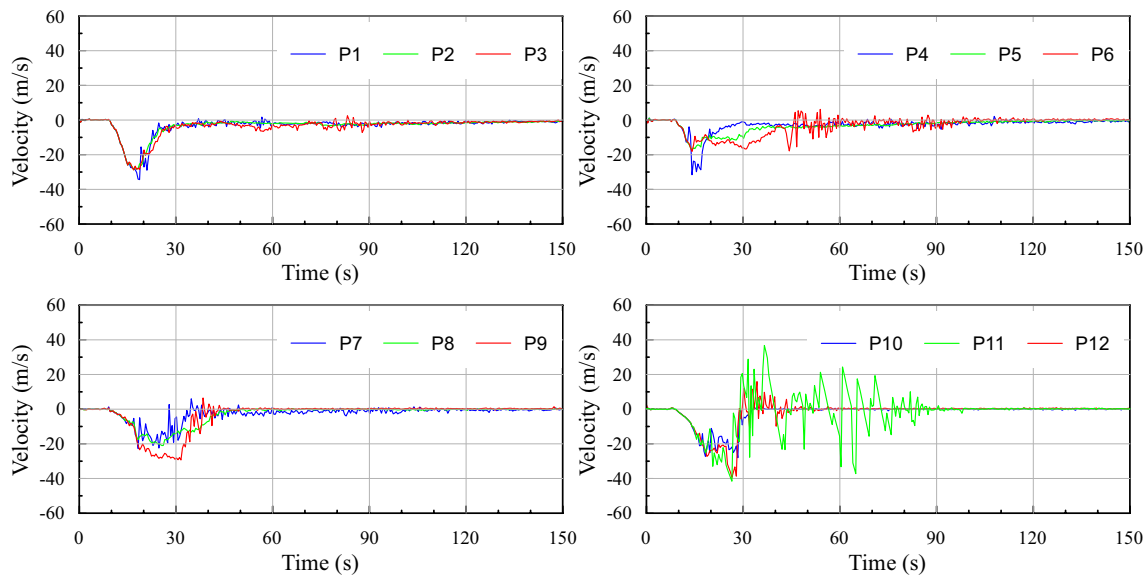


**Fig. 17** Variations of velocity in  $y$  (vertical) direction with time

In the  $x$  direction, the maximum velocities on the surface of the slope prior to the failure were 1.9 m/s (point 3), 1.8 m/s (point 6), 2.0 m/s (point 9), and 1.3 m/s (point 12). Upon failure, the maximum velocities for the front, middle, and rear parts occurred at elapsed times of 20.1 s (about 15.2 m/s), 18.3 s (about 34.9 m/s), and 27.4 s (about 63.6 m/s), respectively (Fig. 16). In the  $y$  direction, a negative velocity indicated a downward motion of the sliding mass, and vice versa (Lo et al. 2011; Li et al. 2012b). The maximum velocities on the surface of the slope before the failure were 1.3 m/s (point 3), 0.9 m/s (point 6), 1.1 m/s (point 9), and 1.3 m/s (point 12), while the maximum velocities for the front, middle, and rear parts after the failure occurred at elapsed times of 18.8 s (about 34.4 m/s), 14.2 s (about 31.6 m/s), and 26.5 s (about 41.2 m/s), respectively (Fig. 17). For all the monitoring points, the velocities in both the  $x$  and  $y$  directions increased steadily with little fluctuations (Figs. 16, 17). This showed that gravity was the major force, and the interaction between particles was relatively low. Upon reaching the peak velocity, the velocities decreased with intense fluctuations, and the most intense fluctuations were observed in the front part (Figs. 16, 17). This showed that the collision interaction and friction became predominant when the deceleration was initiated.

The simulated displacements at the monitoring points are presented in Figs. 18 and 19. It showed that the rear and middle parts took a longer time than the front part to reach the final moving distance. The horizontal distances of the rear and middle parts were only slightly longer than the front part, but a more significant variation was observed for the vertical distance.

The maximum velocity of a landslide is significantly affected by its residual friction. The velocities and displacements in the present study were computed based on the residual friction coefficient of 0.2. The analyses suggested that the exact value of the residual friction coefficient could not be calibrated from the available deposits, and there was no further available record, such as the duration of the Hongshiyuan landslide to help in deriving the actual residual friction. For these reasons, it should be noted that there could be some discrepancies between the actual and the computed velocities.

## Conclusion

Based on the available field data, the kinematic behavior of the Mw 6.5 Ludian earthquake-triggered Hongshiyuan landslide was analyzed using the discrete element method. The material compositions of the landslide dam were interpreted to facilitate evaluations of slope stability and internal stability of the landslide dam.

The simulation results showed that for the landslide sitting in a deep V-shaped valley with constrained movement and steep slip surface gradient, the bond strength (strength of the intact rock mass) played a more influential role than the residual friction coefficient (residual friction between detached rock mass) in the kinematic behavior of the landslide. The effect of residual friction coefficient on the deposition under these circumstances was less significant as compared with most of the previous reported earthquake-triggered landslides.

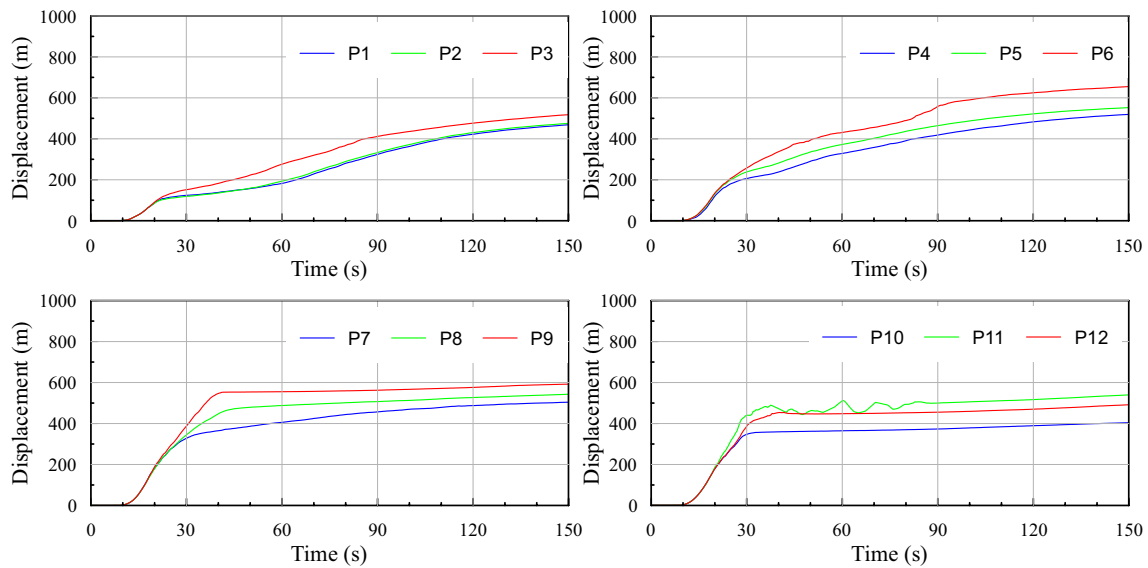


**Fig. 18** Variations of displacement in  $x$  (horizontal) direction with time

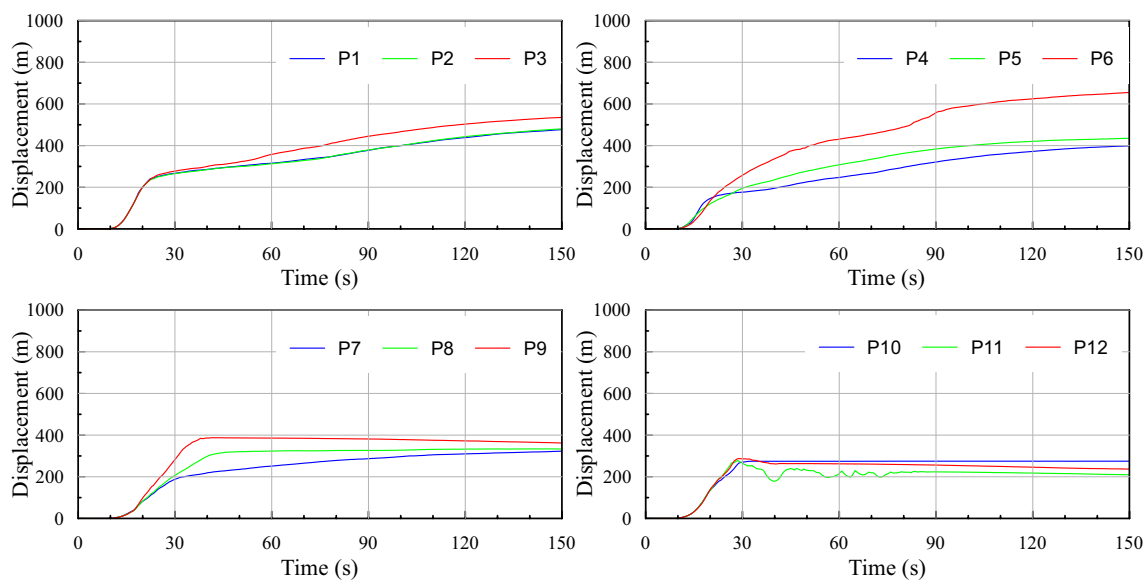


**Fig. 19** Variations of displacement in  $y$  (vertical) direction with time

The simulation results also showed that the rock blocks were scarcely decomposed during sliding. The decomposition of the detached mass was mainly controlled by the development of joints and fissures. The original locations of the depositions can be predicted by simulation, and the grain size distribution can be deduced qualitatively according to the development of the joints and fissures prior to the failure.

This case study proved that, with a proper field data calibration, discrete element method can be a powerful tool to investigate the dynamic process of a landslide. The simulation was useful for understanding the material

compositions of the landslide dam, especially for the materials which were deeply buried and difficult to be extracted from site investigations.

It should also be noted that there were limitations associated with the 2D modeling, such as the lateral spreading of the deposition was neglected, and it was difficult to present the grain size distribution quantitatively. A more complex 3D modeling is recommended for improving the results with the consideration of lateral spreading during the deposition processes.



**Acknowledgements** The authors would like to acknowledge the financial supports from the National Key Research and Development Program of China (Grants 2018YFC1505004 and 2017YFC0404803), National Natural Science Foundation of China (Grant 41571012), and State Key Laboratory of Simulation and Regulation of Water Cycle in River Basin (SKL2018ZY09).

## References

- Avouac J-P, Meng L, Wei S, Wang T, Ampuero J-P (2015) Lower edge of locked Main Himalayan Thrust unzipped by the 2015 Gorkha earthquake. *Nat Geosci* 8:701–711
- Casagli N, Ermini L (1999) Geomorphic analysis of landslide dams in the Northern Apennine. *Jpn Geomorphol Union Trans* 20(3):219–249
- Casagli N, Ermini L, Rosati G (2003) Determining grain size distribution of the material composing landslide dams in the Northern Apennines: sampling and processing methods. *Eng Geol* 69(1):83–97
- Chang KT, Lin ML, Chien CH (2012) The Hungtsaping landslides: from ancient to recent. *Landslides* 9(2):205–214
- Chang ZF, Chen XL, An XW, Cui JW (2016) Contributing factors to the failure of an unusually large landslide triggered by the 2014 Ludian, Yunnan, China, Ms = 6.5 earthquake. *Nat Hazards Earth Syst Sci* 16(2):497–507
- Chen X, Zhou Q, Liu C (2015) Distribution pattern of coseismic landslides triggered by the 2014 Ludian, Yunnan, China Mw 6.1 earthquake: special controlling conditions of local topography. *Landslides* 12:1159–1168
- Costa JE, Schuster RL (1988) The formation and failure of natural dams. *Geol Soc Am Bull* 100(7):1054–1068
- Crosta GB, Chen H, Lee CF (2004) Replay of the 1987 Val Pola Landslide, Italian Alps. *Geomorphology* 60(1):127–146
- Cundall PA (1971) A computer model for simulating progressive, large-scale movements in blocky rock systems. *Proc Symp Int Soc Rock Mech* 1:11–18
- Cundall PA, Strack ODL (1979) A discrete numerical model for granular assemblies. *Geotechnique* 29(1):47–65
- Deng Q, Gong L, Zhang L, Yuan R, Xue Y, Geng X, Hu S (2017) Simulating dynamic processes and hypermobility mechanisms of the Wenjiagou rock avalanche triggered by the 2008 Wenchuan earthquake using discrete element modelling. *Bull Eng Geol Environ* 76(3):923–936
- Fang LH, Wu JP, Wang WL, Lv ZY, Wang CZ, Yang T, Zhong SJ (2014) Relocation of the aftershock sequence of the Ms 6.5 Ludian earthquake and its seismogenic structure. *Seismol Geol* 36(4):1173–1185
- Havenith HB, Strom A, Calvetti F, Jongmans D (2003) Seismic triggering of landslides. Part B: simulation of dynamic failure processes. *Nat Hazards Earth Syst Sci* 3(6):663–682
- Huang D, Cen D, Ma G, Huang R (2015) Step-path failure of rock slopes with intermittent joints. *Landslides* 12(5):911–926
- Itasca (2015) PFC2D particle flow code in 2 dimensions. User's guide. Minneapolis
- Jibson RW (2011) Methods for assessing the stability of slopes during earthquakes—a retrospective. *Eng Geol* 122(1–2):43–50
- Kaneda H, Nakata T, Tsutsumi H, Kondo H, Sugito N, Awata Y, Akhtar SS, Majid A, Khattak W, Awan AA (2008) Surface rupture of the 2005 Kashmir, Pakistan, earthquake and its active tectonic implications. *Bull Seismol Soc Am* 98(2):521–557
- Kargel JS, Leonard GJ, Shugar DH, Haritashya UK, Bevington A, Fielding EJ, Fujita K, Geertsema M, Miles ES, Steiner J, Anderson E, Bajracharya S, Bawden GW, Breashears DF, Byers A, Collins B, Dhital MR, Donnellan A, Evans TL, Geai ML, Glasscoe MT, Green D, Gurung DR, Heijnen R, Hilborn A, Hudnut K, Huyck C, Immerzeel WW, Jiang L, Jibson R, Kääb A, Khanal NR, Kirschbaum D, Kraaijenbrink PDA, Lamsal D, Liu S, Lv M, McKinney D, Nahirnick NK, Nan Z, Ojha S, Olsenholler J, Painter TH, Pleasants M, Pratima KC, Qi Y, Raup BH, Regmi D, Rounce DR, Sakai A, Shangguan D, Shea JM, Shrestha AB, Shukla A, Stumm D, van der Kooij M, Voss K, Wang X, Weihs B, Wolfe D, Wu L, Yao X, Yoder MR, Young N (2016) Geomorphic and geologic controls of geohazards induced by Nepal's 2015 Gorkha earthquake. *Science* 351(6269):aac8353
- Kunming Engineering Corporation Limited (KECL), Zhaotong Investigation, Design & Research Institute of Water Conservancy & Hydropower (Zhaotong Water Survey) (2014) Feasibility study report of rehabilitation project for Hongshiyuan dammed lake. **(Report in Chinese)**
- Li X, He S, Luo Y, Wu Y (2012a) Simulation of the sliding process of Donghekou landslide triggered by the Wenchuan earthquake using a distinct element method. *Environ Earth Sci* 65(4):1049–1054
- Li WC, Li HJ, Dai FC, Lee ML (2012b) Discrete element modeling of a rainfall-induced flowslide. *Eng Geol* 149–150:22–34
- Li S-Q, Guo J-H, Yang X-Y, Li C-Z, Chang X-X (2015a) Causes for the collapse forming Hongshiyuan quake lake. *J Geol Hazards Environ Preserv* 26(3):6–10 **(in Chinese)**
- Li X, Xu X, Ran Y, Cui J, Xie Y, Xu F (2015b) Compound fault rupture in the 2014 Ms 6.5 Ludian, China, earthquake and significance to disaster mitigation. *Seismol Res Lett* 86(3):764–774
- Liu C, Ge Y, Jia X, Guo Y (2016) Dynamic analysis of the Hongshiyuan collapse triggered by Ludian earthquake. *J Disaster Prev Mitig Eng* 36(4):601–608 **(in Chinese)**
- Lo CM, Lin ML, Tang CL, Hu JC (2011) A kinematic model of the Hsiaolin landslide calibrated to the morphology of the landslide deposit. *Eng Geol* 123:22–39
- Lu CY, Tang CL, Chan YC, Hu JC, Chi CC (2014) Forecasting landslide hazard by the 3D discrete element method: a case study of the unstable slope in the Lushan hot spring district, central Taiwan. *Eng Geol* 183(31):14–30
- Lv Q, Liu Y, Yang Q (2017) Stability analysis of earthquake-induced rock slope based on back analysis of shear strength parameters of rock mass. *Eng Geol* 228(13):39–49
- Molnar P, Tapponnier P (1975) Cenozoic tectonics of Asia: effects of a continental collision. *Science* 189(4201):419–426
- Newmark NM (1965) Effects of Earthquakes on Dams and Embankments. *Géotechnique* 15(2):139–160
- Okeke AC, Wang F, Mitani Y (2014) Influence of geotechnical properties on landslide dam failure due to internal erosion and piping. *Landslide science for a safer geoenvironment*. Springer, Berlin, pp 623–631
- Owen LA, Kamp U, Khattak GA, Harp EL, Keefer DK, Bauer MA (2008) Landslides triggered by the 8 October 2005 Kashmir earthquake. *Geomorphology* 94(1–2):1–9
- Pirulli M, Bristeau MO, Mangeney A, Scavia C (2007) The effect of the earth pressure coefficients on the runoff of granular material. *Environ Model Softwre* 22(10):1437–1454
- Poisel R, Preh A (2008) Modifications of PFC3D for rock mass fall modeling. In: Hart R, Detournay C, Cundall P (eds) *Continuum and distinct element numerical modeling in geo-engineering - 2008*. Itasca Consulting Group, Inc., Minneapolis
- Potyondy DO, Cundall PA (2004) A bonded-particle model for rock. *Int J Rock Mech Min Sci* 41(8):1329–1364
- Scaringi G, Fan X, Xu Q, Liu C, Ouyang C, Domènech G, Yang F, Dai L (2018) Some considerations on the use of numerical methods to simulate past landslides and possible new failures: the case of the recent Xinmo landslide (Sichuan, China). *Landslides* 15(7):1359–1375
- Shi ZM, Xiong X, Peng M, Zhang LM, Xiong YF, Chen HX, Zhu Y (2017) Risk assessment and mitigation for the Hongshiyuan

- landslide dam triggered by the 2014 Ludian earthquake in Yunnan, China. *Landslides* 14:269–285
- Soga K, Alonso E, Yerro A, Kumar K, Bandara S (2016) Trends in large-deformation analysis of landslide mass movements with particular emphasis on the material point method. *Géotechnique* 66(3):248–273
- Staron L (2008) Mobility of long-runout rock flows: a discrete numerical investigation. *Geophys J Int* 172(1):455–463
- Swanson FJ, Oyagi N, Tominaga M (1986) Landslide dams in Japan. *Landslide Dams: Processes, risk, and mitigation*. pp 131–145
- Tang C-L, Hu J-C, Lin M-L, Angelier J, Lu C-Y, Chan Y-C, Chu H-T (2009) The Tsaoling landslide triggered by the Chi-Chi earthquake, Taiwan: insights from a discrete element simulation. *Eng Geol* 106(1):1–19
- Tapponnier P, Molnar P (1977) Active faulting and tectonics in China. *J Geophys Res* 82(20):2905–2930
- Tapponnier P, Peltzer G, Armijo R (1986) On the mechanics of the collision between India and Asia. *Geol Soc Lond Spec Publ* 19(1):113–157
- Tapponnier P, Xu ZQ, Roger F, Meyer B, Arnaud N, Wittlinger G, Yang JS (2001) Oblique stepwise rise and growth of the Tibet Plateau. *Science* 294(5547):1671–1677
- Teufelsbauer H, Wang Y, Chiou MC, Wu W (2009) Flow-obstacle interaction in rapid granular avalanches: DEM simulation and comparison with experiment. *Granul Matter* 11(4):209–220
- Tian Y, Xu C, Xu X, Chen J (2016) Detailed inventory mapping and spatial analyses to landslides induced by the 2013 Ms 6.6 Minxian earthquake of China. *J Earth Sci* 27(6):1016–1026
- Wang L, Li S, Yu S, Du X, Deng G (2015) Key techniques for the emergency disposal of Hongshiyuan landslide dam. *J China Inst Water Resour Hydropower Res* 13(4):284–289 (in Chinese)
- Wasowski J, Keefer DK, Lee CT (2011) Toward the next generation of research on earthquake-induced landslides: current issues and future challenges. *Eng Geol* 122(1–2):1–8
- Wu Jian-Hong, Lin Jeen-Shang, Chen Chao-Shi (2009) Dynamic discrete analysis of an earthquake-induced large-scale landslide. *Int J Rock Mech Min Sci* 46(2):397–407
- Xu X, Wen X, Yu G, Chen G, Klinger Y, Hubbard J, Shaw J (2009) Coseismic reverse-and oblique-slip surface faulting generated by the 2008 Mw 7.9 Wenchuan earthquake, China. *Geology* 37(6):515–518
- Xu X, Wen X, Han Z, Chen G, Li C, Zheng W, Zhang S, Ren Z, Xu C, Tan X, Wei Z, Wang M, Ren J, He Z, Liang M (2013) Lushan Ms 7.0 earthquake: a blind reserve-fault event. *Chin Sci Bull* 58(28–29):3437–3443
- Xu C, Xu X, Shen L, Dou S, Wu S, Tian Y, Li X (2014a) Inventory of landslides triggered by the 2014 Ms 6.5 Ludian earthquake and its implications on several earthquake parameters. *Seismol Geol* 36(4):1186–1203
- Xu C, Xu X, Shyu JBH, Zheng W, Min W (2014b) Landslides triggered by the 22 July 2013 Minxian-Zhangxian, China, Mw 5.9 earthquake: inventory compiling and spatial distribution analysis. *J Asian Earth Sci* 92:125–142
- Xu C, Xu X, Yao X, Dai F (2014c) Three (nearly) complete inventories of landslides triggered by the May 12, 2008 Wenchuan Mw 7.9 earthquake of China and their spatial distribution statistical analysis. *Landslides* 11(3):441–461
- Xu C, Xu X, Shyu JBH, Gao M, Tan X, Ran Y, Zheng W (2015a) Landslides triggered by the 20 April 2013 Lushan, China, Mw 6.6 earthquake from field investigations and preliminary analyses. *Landslides* 12(2):365–385
- Xu C, Xu X, Shyu JBH (2015b) Database and spatial distribution of landslides triggered by the Lushan, China Mw 6.6 earthquake of 20 April 2013. *Geomorphology* 248:77–92
- Xu X, Xu C, Li X, Yu G, Wu X, Jiang G (2015c) The Ludian Mw 6.2 earthquake: a minimum earthquake with primary surface ruptures in the eastern Tibetan Plateau. *Seismol Res Lett* 86(6):1622–1635
- Xu C, Xu X, Tian Y, Shen L, Yao Q, Huang X, Ma J, Chen X, Ma S (2016a) Two comparable earthquakes produced greatly different coseismic landslides: the 2015 Gorkha, Nepal and 2008 Wenchuan, China events. *J Earth Sci* 27(6):1008–1015
- Xu X, Han Z, Yang X, Zhang S, Yu G, Zhou B, Li F, Ma B, Chen G, Ran Y (2016b) Seismotectonic map in China and its adjacent regions. *Seismological Press, Beijing*
- Xu X, Sun Q, Jin F, Soga K (2017) Three-dimensional simulation of the Hongshiyuan landslide with the material point method. In: *JTC1 workshop on advances in landslide understanding*
- Yuan RM, Tang CL, Hu JC, Xu X (2014) Mechanism of the Donghekou landslide triggered by the 2008 Wenchuan Earthquake revealed by discrete element modeling. *Nat Hazards Earth Syst Sci* 14(5):1195–1205
- Zhang GW, Lei JS, Liang SS, Sun CQ (2014a) Relocations and focal mechanism solutions of the 3 August 2014 Ludian, Yunnan Ms 6.5 earthquake sequence. *Chin J Geophys* 57(9):3018–3027
- Zhang Y, Xu LS, Chen YT, Liu RF (2014b) Rupture process of the 3 August 2014 Ludian, Yunnan, Mw 6.1 (Ms 6.5) earthquake. *Chin J Geophys* 57(9):3052–3059
- Zhang M, Wu L, Zhang J, Li L (2019) The 2009 Jiweishan rock avalanche, Wulong, China: deposit characteristics and implications for its fragmentation. *Landslides* 16(5):893–906
- Zhao T, Crosta GB (2018) On the dynamic fragmentation and lubrication of coseismic landslides. *J Geophys Res Solid Earth* 123:9914–9932
- Zhou JW, Cui P, Fang H (2013a) Dynamic process analysis for the formation of Yangjiagou landslide-dammed lake triggered by the Wenchuan earthquake, China. *Landslides* 10(3):331–342
- Zhou JW, Cui P, Yang XG (2013b) Dynamic process analysis for the initiation and movement of the Donghekou landslide-debris flow triggered by the Wenchuan earthquake. *J Asian Earth Sci* 76(S1):70–84
- Zhou J, Peng Y, Ming H (2016) Landslides triggered by the 3 August 2014 Ludian earthquake in China: geological properties, geomorphologic characteristics and spatial distribution analysis. *Geomat Nat Hazards Risk* 7(4):1219–1241

**Publisher's Note** Springer Nature remains neutral with regard to jurisdictional claims in published maps and institutional affiliations.